acta physica slovaca vol. 55 No. 2, 181 – 196 **April 2005**

HALO FORMATION IN NEUTRON RICH Ca NUCLEI

M. Kaushik, D. Singh, H. L. Yadav [1]
Department of Physics, Rajasthan University, Jaipur 302004, India

Received 22 April 2004, accepted 6 December 2004

We have investigated the halo formation in the neutron rich Ca isotopes within the framework of recently proposed relativistic mean-field plus BCS (RMF+BCS) approach wherein the single particle continuum corresponding to the RMF is replaced by a set of discrete positive energy states for the calculation of pairing energy. For the neutron rich Ca isotopes in the vicinity of neutron drip-line, it is found that further addition of neutrons causes a rapid increase in the neutron rms radius with a very small increase in the binding energy, indicating thereby the occurrence of halos. This is essentially caused by the gradual filling in of the loosely bound $3s_{1/2}$ state. Interesting phenomenon of accommodating several additional neutrons with almost negligible increase in binding energy is shown to be due to the pairing correlations.

PACS: 21.10.-k, 21.10Ft, 21.10.Dr, 21.10.Gv

1 Introduction

The availability of radioactive beam facilities has generated a spurt of activity devoted to the investigation of exotic drip line nuclei. The neutron rich nuclei away from the line of β-stability with unusually large isospin value are known to exhibit several interesting features. For nuclei close to the neutron drip-line, the neutron density distribution shows a much extended tail with a diffused neutron skin while the Fermi level lies close to the single particle continuum [1]. In some cases it may even lead to the phenomenon of neutron halo, as observed in the case of light nuclei [1–4] , made of several neutrons outside a core with separation energy of the order of $\approx$ 100 keV or less. Interestingly, a theoretical discussion on the possibility of occurrence of such structures has been considered by Migdal [5] already in early 70's. Obviously for such nuclei, due to the weak binding and large spatial dimension of the outermost nucleons, the role of continuum states and their coupling to the bound states become exceedingly important, especially for the pairing energy contribution to the total binding energy of the system. Theoretical investigations of such neutron rich nuclei have been carried out extensively within the framework of mean field theories [6–11] and also employing their relativistic counterparts [3, 12–32].

[1] E-mail address: hlyadav@sancharnet.in

Recently the effect of continuum on the pairing energy contribution has been studied by Grasso *et al*. [11] and Sandulescu *et al*. [10] within the HF+BCS+Resonant continuum approach. Similarly the effect of inclusion of positive energy resonant states on the pairing correlations has been investigated by Yadav et al. [30]. A detailed comparative study of the Hartree-Fock-Bogoliubov (HFB) approach with those of the HF+BCS+Resonant continuum calculations carried out by Grasso *et al*. [11] and Sandulescu *et al*. [10] has provided useful insight to the validity of different approaches for the treatment of drip-line nuclei. The interesting result of these investigation is that only a few low energy resonant states, especially those near the Fermi surface influence in an appreciable way the pairing properties of nuclei far from the β-stability. This finding is of immense significance because one can eventually make use of this for systematic studies of a large number of nuclei by employing a simpler HF+BCS approximation. Amongst the mean-field theoretic treatments, however, currently the relativistic mean field (RMF) theory is being extensively used for the study of unstable nuclei [3, 18–25]. The advantage of the RMF approach is that it provides the spin-orbit interaction in the entire mass region in a natural way [12–14]. This indeed has proved to be very crucial for the study of unstable nuclei near the drip line, since the single particle properties near the threshold are prone to large changes as compared to the case of deeply bound levels in the nuclear potential. In addition to this, the pairing properties are equally important for nuclei near the drip line. In order to take into account the pairing correlations together with a realistic mean field, the framework of standard RHB approach is commonly used [24, 26]. In this connection, the finding above for the non-relativistic frameworks has turned out to be very important for the systematic work of unstable nuclei in the relativistic approach. This has been demonstrated recently by Yadav et al. [30, 31] for the chains of $^{48-98}\mathrm{Ni}$ and $^{96-176}\mathrm{Sn}$ isotopes covering the drip lines. Indeed the RMF+BCS scheme [30,31] wherein the single particle continuum corresponding to the RMF is replaced by a set of discrete positive energy states yields results which are found to be in close agreement with the experimental data and with those of recent continuum relativistic Hartree-Bogoliubov (RCHB) and other similar mean-field calculations [24, 32].

With the success of the RMF+BCS approach for the prototype calculations of Ni and Sn isotopes [30, 31], detailed calculations for the chain of Ca isotopes and also those of O, Ni, Zr, Sn and Pb isotopes using the TMA [21] and the NL-SH [23] force parameterizations have been carried out. The results of these calculations [33] for the two neutron separation energy, neutron, proton, and matter rms radii, and single particle pairing gaps etc., and their comparison with the available experimental data and with the results of other mean-field approaches demonstrate the general validity of the RMF+BCS approach. In this paper, in continuation to our earlier publication [31], we present briefly the results for the chain of Ca isotopes but with a special emphasis on our findings for the possible halo formation in the neutron rich Ca isotopes within the RMF+BCS approach. It is shown that the resonant $1g_{9/2}$ and the $3s_{1/2}$ states which lie close to zero energy in continuum and gradually come down to become bound with increasing neutron number, play the crucial role. Evidently the concentration of the major part of the wave function of the resonant $1g_{9/2}$ state within the potential well and its proximity with the Fermi surface while being close to zero energy together provide a favorable condition for the existence of extremely neutron rich Ca isotopes, whereas the $3s_{1/2}$ state with a well spread wave function, due to the absence of a centrifugal barrier, helps to cause the occurrence of halos. The role of pairing correlations as described here is found to be consistent with the conclusions of non-relativistic HFB studies of neutron rich weakly bound nuclei discussed recently by Bennaceur et al. [4].

2 Theoretical Formulation and Model

Our RMF calculations have been carried out using the model Lagrangian density with nonlinear terms both for the σ and ω mesons as described in detail in Refs. [21]

$$\begin{aligned}
\mathcal{L} &= \bar{\psi}[\imath\gamma^{\mu}\partial_{\mu} - M]\psi \\
&+\frac{1}{2}\,\partial_{\mu}\sigma\partial^{\mu}\sigma - \frac{1}{2}m_{\sigma}^{2}\sigma^{2} - \frac{1}{3}g_{2}\sigma^{3} - \frac{1}{4}g_{3}\sigma^{4} - g_{\sigma}\bar{\psi}\sigma\psi \\
&-\frac{1}{4}H_{\mu\nu}H^{\mu\nu} + \frac{1}{2}m_{\omega}^{2}\omega_{\mu}\omega^{\mu} + \frac{1}{4}c_{3}(\omega_{\mu}\omega^{\mu})^{2} - g_{\omega}\bar{\psi}\gamma^{\mu}\psi\omega_{\mu} \\
&-\frac{1}{4}G_{\mu\nu}^{a}G^{a\mu\nu} + \frac{1}{2}m_{\rho}^{2}\rho_{\mu}^{a}\rho^{a\mu} - g_{\rho}\bar{\psi}\gamma_{\mu}\tau^{a}\psi\rho^{\mu a} \\
&-\frac{1}{4}F_{\mu\nu}F^{\mu\nu} - e\bar{\psi}\gamma_{\mu}\frac{(1-\tau_{3})}{2}A^{\mu}\psi\ , \qquad (1)
\end{aligned}$$

where the field tensors H, G and F for the vector fields are defined by

$$\begin{aligned}
H_{\mu\nu} &= \partial_{\mu}\omega_{\nu} - \partial_{\nu}\omega_{\mu}, \\
G_{\mu\nu}^{a} &= \partial_{\mu}\rho_{\nu}^{a} - \partial_{\nu}\rho_{\mu}^{a} - 2g_{\rho}\,\epsilon^{abc}\rho_{\mu}^{b}\rho_{\nu}^{c}, \\
F_{\mu\nu} &= \partial_{\mu}A_{\nu} - \partial_{\nu}A_{\mu}\ ,
\end{aligned}$$

and other symbols have their usual meaning.

The set of parameters appearing in the effective Lagrangian (1) have been obtained in an extensive study which provides a good description for the ground state of nuclei and that of the nuclear matter properties [21]. This set, termed as TMA, has an A-dependence and covers the light as well as heavy nuclei from ^{16}O to ^{208}Pb. Table 1 lists the TMA set of parameters along with the results for the calculated bulk properties of nuclear matter. As mentioned earlier we have also carried out the RMF+BCS calculations using the NL-SH force parameters [23] in order to compare our results with those obtained in the RCHB calculations [32] using this force parameterizations. The NL-SH parameters are also listed in Table 1 together with the corresponding nuclear matter properties.

Based on the single-particle spectrum calculated by the RMF described above, we perform a state dependent BCS calculations [34, 35]. As we already mentioned, the continuum is replaced by a set of positive energy states generated by enclosing the nucleus in a spherical box. Thus the gap equations have the standard form for all the single particle states, i.e.

$$\Delta_{j_1} = -\frac{1}{2}\frac{1}{\sqrt{2j_1+1}}\sum_{j_2}\frac{\left\langle (j_1{}^2)\,0^{+}\,|V|\,(j_2{}^2)\,0^{+}\right\rangle}{\sqrt{\left(\varepsilon_{j_2}\,-\,\lambda\right)^{2}\,+\,\Delta_{j_2}^{2}}}\ \sqrt{2j_2+1}\ \Delta_{j_2}\ , \qquad (2)$$

where ε_{j_2} are the single particle energies, and λ is the Fermi energy, whereas the particle number condition is given by $\sum_j (2j+1)v_j^2 = \mathrm{N}$. In the calculations we use for the pairing interaction a delta force, i.e., $V = -V_0\delta(r)$ with the same strength V_0 for both protons and neutrons. The value of the interaction strength $V_0 = 350$ MeV fm^3 was determined in ref. [30] by obtaining a best fit to the binding energy of Ni isotopes. We use the same value of V_0 for our present studies

Tab. 1. Parameters of the Lagrangian TMA [21] and NL-SH [23] together with the nuclear matter properties obtained with these effective forces.

Force Parameters			Nuclear Matter Properties		
	TMA	NL-SH		TMA	NL-SH
M (MeV)	938.9	939.0	Saturation density		
m_σ(MeV)	519.151	526.059	ρ_0 (fm)$^{-3}$	0.147	0.146
m_ω(MeV)	781.950	783.0	Bulk binding energy/nucleon		
m_ρ(MeV)	768.100	763.0	$(E/A)_\infty$ (MeV)	16.0	16.346
g_σ	10.055 + 3.050/A$^{0.4}$	10.444	Incompressibility		
g_ω	12.842 + 3.191/A$^{0.4}$	12.945	K (MeV)	318.0	355.36
g_ρ	3.800 + 4.644/A$^{0.4}$	4.383	Bulk symmetry energy/nucleon		
g_2 (fm)$^{-1}$	-0.328 - 27.879/A$^{0.4}$	-6.9099	a_{sym} (MeV)	30.68	36.10
g_3	38.862 - 184.191/A$^{0.4}$	-15.8337	Effective mass ratio		
c_3	151.590 - 378.004/A$^{0.4}$		m*/m	0.635	0.60

of isotopes of other nuclei as well. Apart from its simplicity, the applicability and justification of using such a δ-function form of interaction has been recently discussed in Refs. [6] and [8], whereby it has been shown in the context of HFB calculations that the use of a delta force in a finite space simulates the effect of finite range interaction in a phenomenological manner (see also [36] and [37] for more details). The pairing matrix element for the δ-function force is given by

$$\left\langle (j_1{}^2)\, 0^+ \,|V|\, (j_2{}^2)\, 0^+ \right\rangle \;=\; -\frac{V_0}{8\pi}\sqrt{(2j_1+1)(2j_2+1)}\; I_R \;, \tag{3}$$

where I_R is the radial integral having the form

$$I_R \;=\; \int dr \frac{1}{r^2}\left(G^\star_{j_1}\, G_{j_2} \,+\, F^\star_{j_1}\, F_{j_2}\right)^2 . \tag{4}$$

Here G_α and F_α denote the radial wave functions for the upper and lower components, respectively, of the nucleon wave function expressed as

$$\psi_\alpha = \frac{1}{r}\begin{pmatrix} i\;G_\alpha\;\mathcal{Y}_{j_\alpha l_\alpha m_\alpha} \\ F_\alpha\,\sigma\cdot\hat{r}\;\mathcal{Y}_{j_\alpha l_\alpha m_\alpha}\end{pmatrix} , \tag{5}$$

and satisfy the normalization condition

$$\int dr\,\{|G_\alpha|^2 \,+\, |F_\alpha|^2\} \,=\, 1. \tag{6}$$

In Eq. (5) the symbol $\mathcal{Y}_{jlm}$ has been used for the standard spinor spherical harmonics with the phase i^l. The coupled field equations obtained from the Lagrangian density in (1) are finally reduced to a set of simple radial equations [14] which are solved self consistently along with the equations for the state dependent pairing gap Δ_j and the total particle number N for a given nucleus.

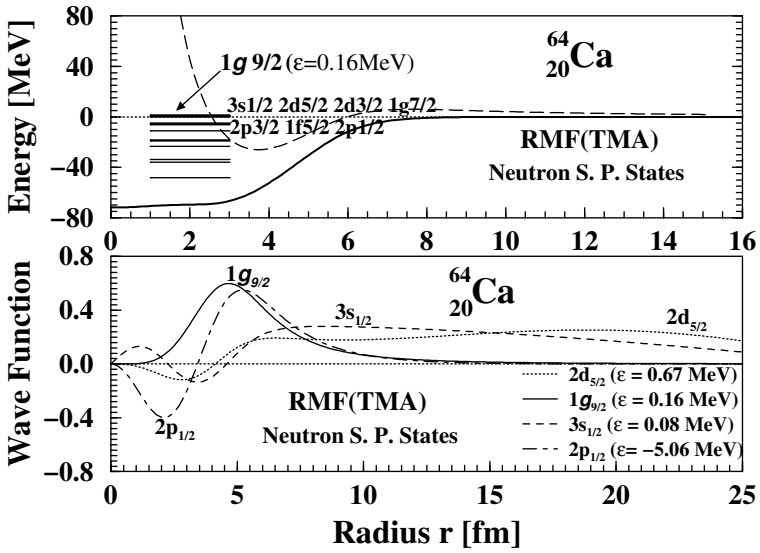

Fig. 1. Upper panel: The RMF potential energy (sum of the scalar and vector potentials), for the nucleus ^{64}Ca shown by the solid line as a function of radius r. The long dashed line represents the sum of RMF potential energy and the centrifugal barrier energy for the neutron resonant state $1g_{9/2}$. It also shows the energy spectrum of some important neutron single particle states along with the resonant $1g_{9/2}$ state at 0.16 MeV. Lower panel: Radial wave functions of a few representative neutron single particle states with energy close to the Fermi surface for the nucleus ^{64}Ca. The solid line shows the resonant $1g_{9/2}$ state.

3 Results and Discussion

Our earlier calculations for chains of Ni and Sn isotopes [30, 31] and present investigations of Ca isotopes as well as of other nuclei indicate that the neutron rich Ca isotopes constitute the most interesting example of loosely bound system. For an understanding of such an exotic system the total pairing energy contribution to the binding energy plays a crucial role. This in turn implies the importance of the structure of single particle states near the Fermi level, as the scattering of particles from bound to continuum states and vice versa due to pairing interaction involves mainly these states. The last few occupied states near the Fermi level also provide an understanding of the radii of the loosely bound exotic nuclei. The neutron rich nuclei in which the last filled single particle state near the Fermi level is of low angular momentum ($s_{1/2}$ or $p_{1/2}$ state), especially the $l = 0$ state, can have large radii due to large spatial extension of the $s_{1/2}$ state which has no centrifugal barrier.

In order to demonstrate our results we have chosen ^{64}Ca as a representative example of the neutron rich Ca isotopes. Moreover, since the results obtained with TMA and NL-SH forces are found to be almost similar, to save space we describe in details only the results for the TMA force, whereas the results obtained with the NL-SH force have been discussed at places for the purpose of comparison. The upper panel of Fig. 1 shows the calculated RMF potential, a sum of

scalar and vector potentials, along with the spectrum for the bound neutron single particle states for the neutron rich ^{64}Ca obtained with the TMA force. The figure also shows the positive energy state corresponding to the first low-lying resonance $1g_{9/2}$, and other positive energy states, for example, $3s_{1/2}$, $2d_{5/2}$, $2d_{3/2}$ and $1g_{7/2}$ close to the Fermi surface which play significant role for the binding of neutron rich isotopes through their contributions to the total pairing energy. In contrast to other states in the box which correspond to the non-resonant continuum, the position of the resonant $1g_{9/2}$ state is not much affected by changing the box radius around $R = 30$ fm. We have also depicted in this part of Fig. 1 the total mean field potential for the neutron $1g_{9/2}$ state, obtained by adding the centrifugal potential energy. It is evident from the figure that the effective total potential for the $1g_{9/2}$ state has an appreciable barrier to form a quasi-bound or resonant state. Such a meta-stable state remains mainly confined to the region of the potential well and the wave function exhibits characteristics similar to that of a bound state. This is clearly seen in the lower panel of Fig. 1 which depicts the radial wave functions of some of the neutron single particle states lying close to the Fermi surface, the neutron Fermi energy being $\lambda_n = -0.066$ MeV. These include the bound $2p_{1/2}$, and the continuum $3s_{1/2}$ and $2d_{5/2}$ states in addition to the state corresponding to the resonant $1g_{9/2}$. The wave function for the $1g_{9/2}$ state in Fig. 1 (lower panel) is clearly seen to be confined within a radial range of about 8 fm and has a decaying component outside this region, characterizing a resonant state. In contrast, the main part of the wave function for the non-resonant states, e.g. $2d_{5/2}$, is seen to be mostly spread over outside the potential region. This type of state thus has a poorer overlap with the bound states near the Fermi surface leading to small value for the pairing gap $\Delta_{2d_{5/2}}$. Further, the positive energy states lying much higher from the Fermi level, for example, $1h_{11/2}$, $1i_{13/2}$ etc. have a negligible contribution to the total pairing energy of the system. These features can be seen from Fig. 2 (upper panel) which depicts pairing gap energy Δ_j for the neutron states in ^{64}Ca. The gap energy for the $1g_{9/2}$ state is seen to have a value close to 1 MeV which is quantitatively similar to that of bound states $1f_{7/2}$ and $2p_{3/2}$ etc. The non-resonant states like $3s_{1/2}$ and $2d_{5/2}$ in continuum have much smaller gap energy. However, while approaching the neutron drip line nucleus ^{72}Ca, the single particle states $3s_{1/2}$, $1g_{9/2}$, $2d_{5/2}$ and $2d_{3/2}$ which lie near the Fermi level gradually come down close to zero energy, and subsequently the $1g_{9/2}$ and $3s_{1/2}$ states become bound. This helps in accommodating more and more neutrons with very little binding. In fact, the occupancy of the $3s_{1/2}$ state in these neutron rich isotopes causes the halo formation as will be seen later.

In the lower panel of Fig. 2 we have shown the contribution of pairing energy which plays an important role for the stability of nuclei and consequently in deciding the position of the neutron and proton drip lines. It is seen that the RMF+BCS calculations carried out with two different sets of force parameters, the TMA and NL-SH, yield almost similar results also for the pairing energies. The differences in the two results can be attributed to the difference in the detailed structure of single particle energies obtained with the TMA and NL-SH forces. One observes from Fig. 2 (lower panel) that the pairing energy vanishes for the neutron numbers $N = 14, 20, 28$ and 40 indicating the shell closures. In particular the usual shell closure at $N = 50$ is found to be absent for the neutron rich Ca isotopes and at $N = 40$ a new shell closure appears. This reorganization of single particle energies with large values of N/Z ratio (for the neutron rich Ca isotopes N/Z $\geq$ 2) has its origin in the deviation of the strength of spin-orbit splitting from the conventional shell model results for nuclei with not so large N/Z ratio.

The results for the ground state properties including the binding energy, two neutron sepa-

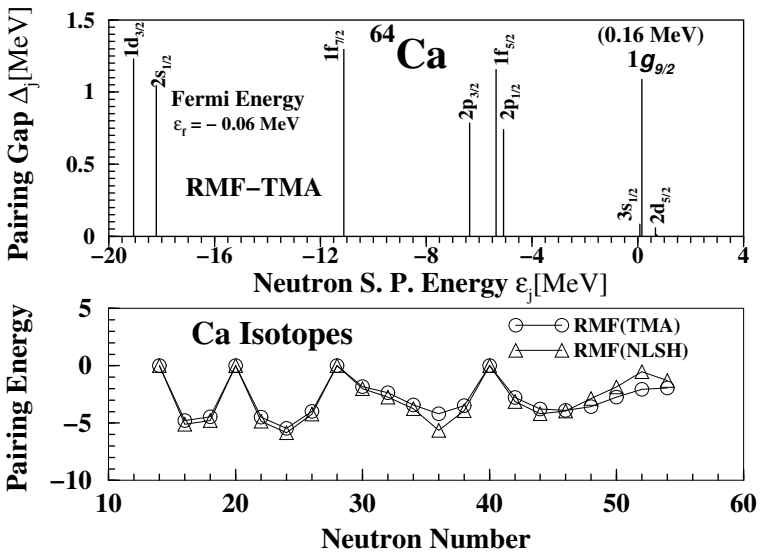

Fig. 2. Upper panel: Pairing gap energy Δ_j of neutron single particle states with energy close to the Fermi surface for the nucleus ^{64}Ca. The resonant $1g_{9/2}$ state at energy 0.165 MeV has the gap energy of about 1 MeV which is close to that of bound states like $1f_{5/2}$, $1f_{7/2}$, $1d_{3/2}$ etc. Lower panel: Pairing energy for the Ca isotopes obtained with the TMA (open circles) and the NL-SH (open triangles) force parameters.

ration energy, and the rms radii for the neutron, proton, matter and charge distributions for the Ca isotopes calculated with the TMA force have been listed in Table 2. The table also lists the available experimental data [38] for the binding energies, two neutron separation energy as well as the binding energy per nucleon (B/A) for the purpose of comparison. The available experimental data for the radii are very sparse and have not been listed. It is interesting to note that the maximum value of B/A occurs for the ^{46}Ca isotope and not the doubly magic isotopes ^{40}Ca or ^{48}Ca. The shell structure as revealed by the pairing energies are also exhibited in the variation of two neutron separation energies S_{2n} as shown in the lower panel of Fig. 3. An abrupt increase in the S_{2n} values for the isotopes next to magic numbers is clearly seen. This part of the figure also depicts the results of two neutron separation energy obtained in the RCHB approach and their comparison with available experimental data. The upper panel of Fig. 3 depicts the difference between the experimental and calculated values. It is seen that the TMA and NL-SH forces yield similar results and the isotopes beyond A=66 have two neutron separation energy close to zero. The two neutron drip line is found to occur at A=70 (N=50) and A=72 (N=52) for the TMA and NL-SH forces, respectively. The isotopes with mass number $70 < A < 76$ for the TMA, and those with $72 < A < 76$ for the NL-SH case are found to be just unbound with negative separation energy very close to zero. Accordingly in Fig. 3 we have shown the results up to N=56 to emphasize this point. Also, for our purpose we shall neglect this small difference in the position of drip line mentioned above. The similarity of different calculated results amongst themselves and their satisfactory comparison with data are well demonstrated in the upper panel.

Tab. 2. Results for the ground state properties of Ca-isotopes calculated with the TMA force parameter set. Listed are the total binding energy, BE, the two neutron separation energy, S_{2n}, binding energy per nucleon, B/A, and neutron, proton, matter and charge root mean square radii denoted by r_n, r_p, r_m, r_c, respectively. The available experimental data [38] on the binding energy, $(BE)_{exp}$, and that of $(S_{2n})_{exp}$ and $(B/A)_{exp}$ are also listed for comparison.

Nucleus	$(BE)_{exp}$ MeV	BE MeV	$(S_{2n})_{exp}$ MeV	S_{2n} MeV	$(B/A)_{exp}$ MeV	B/A MeV	r_n fm	r_p fm	r_m fm	r_c fm
^{34}Ca	245.625	246.684			7.224	7.255	3.039	3.415	3.266	3.511
^{36}Ca	281.360	280.968	35.735	34.284	7.816	7.805	3.168	3.394	3.296	3.489
^{38}Ca	313.122	313.114	31.762	32.146	8.240	8.240	3.262	3.385	3.327	3.479
^{40}Ca	342.052	343.208	28.930	30.094	8.551	8.580	3.337	3.383	3.360	3.475
^{42}Ca	361.895	363.843	19.843	20.635	8.617	8.663	3.426	3.381	3.404	3.471
^{44}Ca	380.960	382.823	19.065	18.980	8.658	8.700	3.501	3.382	3.447	3.471
^{46}Ca	398.769	400.385	17.809	17.562	8.669	8.704	3.565	3.386	3.488	3.473
^{48}Ca	415.991	416.629	17.222	16.244	8.666	8.680	3.621	3.391	3.527	3.476
^{50}Ca	427.491	425.235	11.500	8.606	8.550	8.505	3.759	3.412	3.624	3.495
^{52}Ca	436.600	433.287	9.109	8.052	8.396	8.332	3.872	3.435	3.710	3.516
^{54}Ca	443.800	440.711	7.200	7.424	8.219	8.161	3.966	3.463	3.788	3.542
^{56}Ca	449.600	448.148	5.800	7.437	8.029	8.003	4.082	3.493	3.882	3.569
^{58}Ca		455.380		7.232		7.851	4.115	3.522	3.921	3.596
^{60}Ca		462.135		6.755		7.702	4.173	3.551	3.977	3.623
^{62}Ca		462.704		0.569		7.463	4.248	3.573	4.042	3.643
^{64}Ca		462.964		0.260		7.234	4.361	3.593	4.137	3.662
^{66}Ca		463.032		0.068		7.016	4.634	3.609	4.349	3.675
^{68}Ca		463.058		0.026		6.810	4.851	3.623	4.525	3.687
^{70}Ca		463.075		0.017		6.615	4.926	3.640	4.596	3.703
^{72}Ca		462.972		-0.103		6.430	5.007	3.655	4.671	3.716

The rms radii for the proton and neutron , $r_{p,n} = (\langle r^2_{p(n)} \rangle)^{1/2}$ have been calculated from the respective density distributions. The experimental data for the rms charge radii are used to deduce the nuclear rms proton radii using the relation $r_c^2 = r_p^2 + 0.64\, fm^2$ for the purpose of comparison. In the middle panel of Fig. 4 we have shown the RMF+BCS results for the neutron and proton rms radii for the NL-SH force along with the RCHB results [32] also obtained using the NL-SH force for the purpose of comparison. These results are quite similar as can be seen from the differences plotted in the upper panel. The experimental data for the proton and neutron rms radii are available only for a few stable Ca isotopes. The lower panel of Fig. 4 depicts a comparison of the RMF+BCS results using the TMA force with the available experimental data. It is seen from Fig. 4 that the measured proton radii r_p for the isotopes $^{40-48}$Ca are in excellent agreement with our RMF+BCS results. Similarly the neutron radii r_n for the ^{40,42,44,48}Ca isotopes are found to compare quite well as has been depicted in the lower panel of Fig. 4.

As described earlier, in the case of neutron rich Ca isotopes the neutron $1g_{9/2}$ state happens to be a resonant state having good overlap with the bound states near the Fermi level. This causes the pairing interaction to scatter particles from the neighboring bound states to the resonant state and vice versa. Thus, it is found that the resonant $1g_{9/2}$ state starts being partially occupied even before the lower bound single particle states are fully filled in. Further, for neutron rich

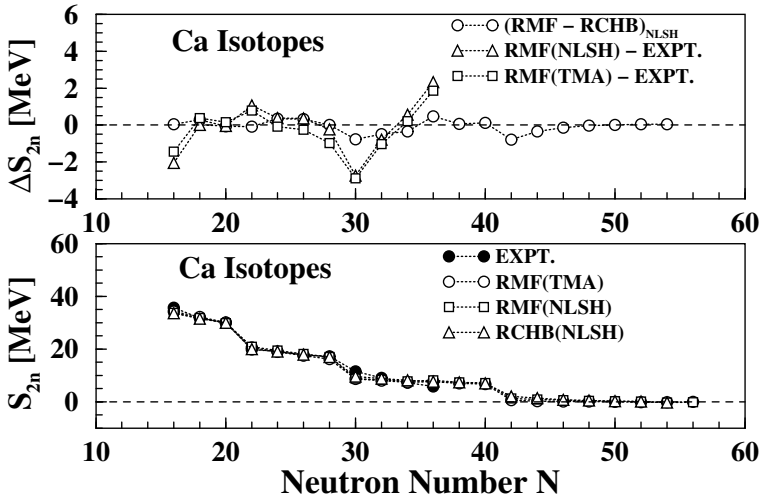

Fig. 3. In the lower panel two neutron separation energies for the Ca isotopes calculated with the TMA (open circles) and the NL-SH (open squares) force parameters are compared with the RCHB calculations of Ref. [32] carried out with the NL-SH force (open triangles) and with the available experimental data [38]. The upper panel shows the difference in the RMF+BCS and the RCHB results as well as the difference between calculated results with respect to the available experimental data [38].

Ca isotopes it is found that the neutron $3s_{1/2}$ state which lies close to the $1g_{9/2}$ state also starts getting partially occupied before the $1g_{9/2}$ state is completely filled. The neutron $3s_{1/2}$ state due to lack of centrifugal barrier contributes more to the neutron rms radius as compared to the $1g_{9/2}$ state, and thus one observes in Fig. 4 (lower panel) a rapid increase in the neutron rms radius beyond the neutron number $N = 42$ indicating the formation of halos. A comparison of the rms neutron radii with the $r_n = r_0 N^{1/3}$ line shown in the figure suggests that these radii for the drip-line isotopes do not follow the $r_0 N^{1/3}$ systematics.

Similar calculations for the neutron radii of Ni and Sn isotopes [30, 31], however, do not exhibit halo formation as can be seen from Fig. 5. As regards the possibility of halo formation in other nuclei, the following remark is pertinent. From our comprehensive calculations of chains of proton magic nuclei [33], it is found that the isotopes of O as well as Pb nuclei also do not exhibit the tendency of halo formations. On the other hand, the proton sub-magic neutron rich Zr isotopes do have a single particle structure that provides a favorable condition for the halos, albeit in a less pronounced manner. In this case the single particle $3p_{1/2}$ state lying close to the continuum threshold plays the crucial role.

An important aspect of the heavy neutron rich nuclei is the formation of the neutron skin. [1] The neutron density distributions in the neutron rich $^{62-72}$Ca nuclei are found to be widely spread out in the space indicating the formation of neutron halos. This has been demonstrated in Fig. 6 which shows the variation in the proton (upper panel) and neutron (lower panel) radial density distributions with increasing neutron number for the TMA force calculations. It may be

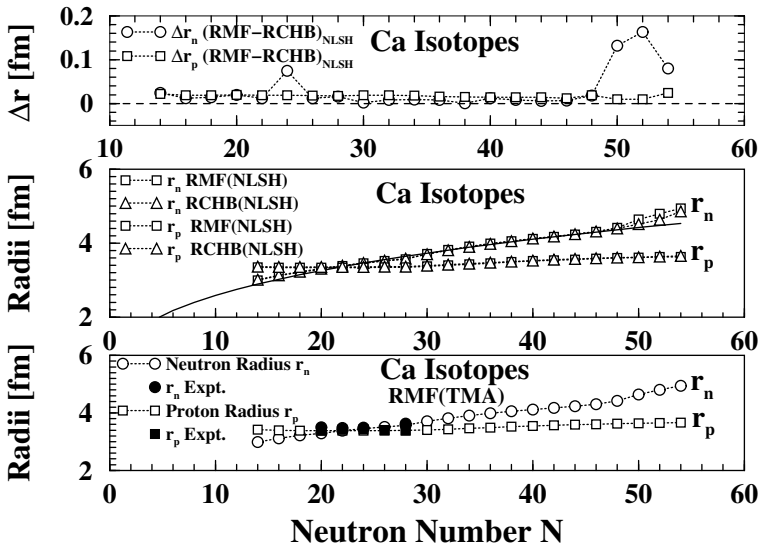

Fig. 4. Lower panel: The rms radii of neutron distribution r_n (open circles), and that of proton distribution r_p (open squares) obtained with the TMA force are compared with the available experimental data [40], shown by solid circles and solid squares, respectively. Middle panel: A comparison of RMF+BCS results (open squares) for rms radii r_n and r_p with that of RCHB (open triangles) from Ref. [32] obtained with the NL-SH force . Upper panel: Difference between the results obtained from RMF+BCS and the RCHB approaches for the rms radii using the NL-SH force shown in the middle panel.

emphasized that the density distributions obtained from the NL-SH force parameterizations are almost similar to those obtained using the TMA force and, therefore, here we have chosen to show only the results for the TMA force.

As depicted in the upper panel of the Fig. 6, the proton distributions are observed to be confined to smaller distances. Moreover, these start to fall off rapidly already at smaller distances (beyond $r > 3$ fm.) as compared to those for the neutron density distributions shown in the lower panel. In the interior as well as at outer distances, as shown in the inset of the upper panel, the proton density values are larger for the proton rich Ca isotopes and decrease with increasing neutron number N. However, in the surface region, ($r \approx 4$ fm), the proton density values reverse their trend and increase with increasing neutron number. Due to this feature of the proton density distributions the proton radii are found to increase, albeit in a very small measure, with increasing neutron number.

Similarly the lower panel of Fig. 6, depicting the neutron density distribution, shows that for the magic numbers N = 14, 20, 28 and 40 the neutron densities fall off rapidly and have smaller tails as compared to the isotopes with other neutron numbers. The density distribution for the N = 50 case is seen to be very different from the above cases indicating thereby that for the neutron rich Ca isotopes the N = 50 does not correspond to a magic number. The neutron densities of the isotopes having $N > 40$ are found to exhibit especially widespread distributions out side the

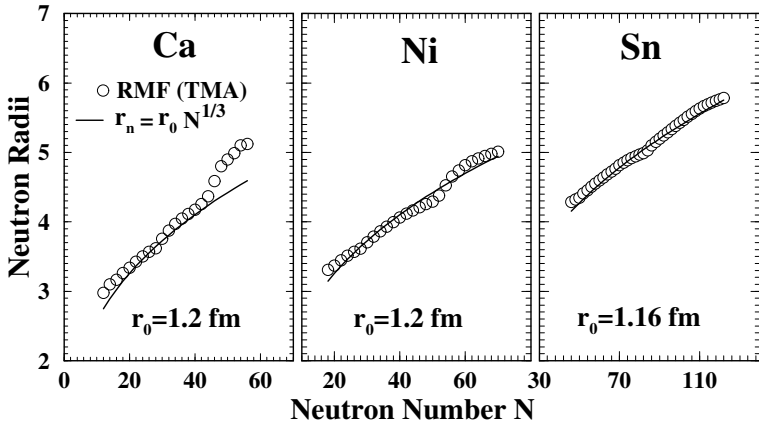

Fig. 5. The RMF results [30, 31, 33] for the neutron rms radii r_n for the isotopes of Ca, Ni and Sn nuclei obtained with the TMA force. These are compared with a rough estimate of neutron distribution radius given by $r_n = r_0 N^{1/3}$ wherein the radius constant r_0 is chosen to provide the best fit to the theoretical results. Halo formation in the case of neutron rich Ca isotopes is clearly seen.

range of the interaction potential. This has been explicitly demonstrated in the inset of lower panel of Fig. 6. Moreover, these results are also found to be very similar to those obtained using the RCHB approach [32]. In particular, for the isotopes with neutron shell closure corresponding to $N = 14$, 20, 28 and 40 this similarity extends up to large radial distances. For the other isotopes, there are small deviations between the RMF+BCS and the RCHB approaches beyond the radial distance $r = 8$ fm. However, beyond this distance the densities are already quite reduced ranging between 10^{-4} fm^{-3} to 10^{-8} fm^{-3}. In Fig. 6 (lower panel) it is interesting to note that the neutron density distributions, out side the nuclear surface and at large distances, for the neutron rich Ca isotopes with neutron number $N \geq 42$ are larger by several orders of magnitude as compared to the lighter isotopes. This behavior of the density distribution for the neutron rich Ca isotopes is quite different from the corresponding results, especially for the neutron rich isotopes of Ni, Sn and Pb nuclei [30, 31, 33]. In the latter cases, as the neutron number is added the tail of the neutron density distributions for the neutron rich isotopes tend to saturate.

The large relative enhancement in the tail region of neutron density distributions of the neutron rich Ca isotopes beyond $N = 40$ (or $A = 60$) gives rise to the halo formation in these isotopes. Essentially, it is caused due to weakly bound neutrons occupying the single particle states near the Fermi level which is itself almost close to zero energy for the neutron rich isotopes as has been shown in Fig. 7. The large energy gaps between single particle levels $1d_{5/2}$ and $1d_{3/2}$ (not shown in Fig. 7), and the levels $2p_{1/2}$ and $3s_{1/2}$ etc. are responsible for the properties akin to shell or sub-shell closures in the $^{34-72}$Ca isotopes for the neutron number N = 14 and 40 apart from the traditional magic nos. N = 20 and 28. However the N = 50 shell closure is found to disappear due to absence of gaps between the $1g_{9/2}$ state and the states in the s-d shell. A better understanding of the halo formation in the neutron rich ($N > 40$) Ca isotopes

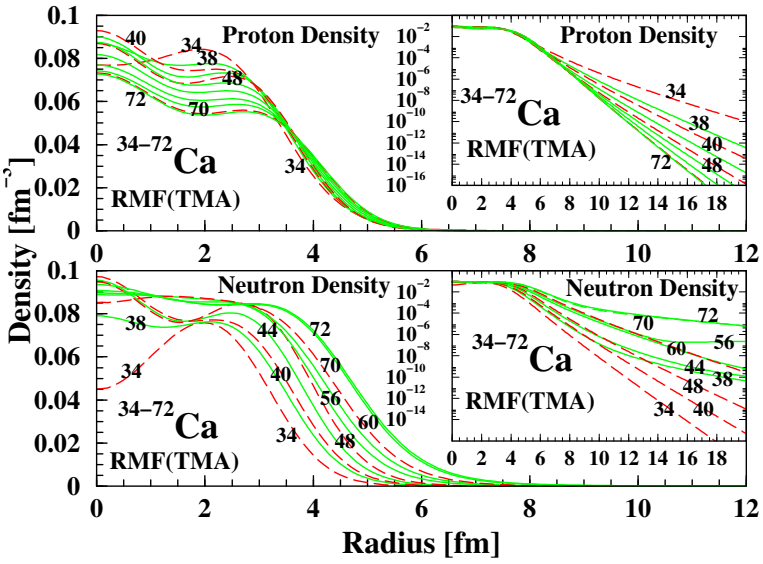

Fig. 6. The upper and lower panels, respectively, show the proton and neutron density distributions for the Ca isotopes obtained with the TMA force. The numbers on the density distribution lines indicate the mass number of the Ca isotope.The insets show the results on a logarithmic scale up to rather large distances.

is rendered if one looks into the detailed features of single particle spectrum and its variation shown in Fig. 7 as one moves from the lighter isotope to heavier one . For example, the neutron Fermi energy which lies at $\epsilon_f = -19.90$ MeV in the neutron deficient ^{34}Ca nucleus moves to $\epsilon_f = -0.21$ MeV in the neutron rich ^{62}Ca, and to $\epsilon_f = 0.08$ MeV (almost at the beginning of the single particle continuum) in ^{70}Ca. The $1g_{9/2}$ state which lies at higher energy in continuum for the lighter isotopes, comes down gradually to become slightly bound for the neutron rich isotopes. Similarly, the $3s_{1/2}$ state which lies in continuum for the lighter isotopes (for example at $\epsilon = 0.70$ MeV in ^{34}Ca) also comes down, though not so drastically, to become slightly bound (($\epsilon = -0.05$ MeV in ^{68}Ca) for the neutron rich isotopes.

In the case of ^{60}Ca with shell closure for both protons and neutrons, the neutron single particle states are filled in up to the $2p_{1/2}$ state, while the next high lying states $3s_{1/2}$ and $1g_{9/2}$, separated by about 5 MeV from the $2p_{1/2}$ level, are completely empty. Now on further addition of 2 neutrons, it is observed that the $1g_{9/2}$ is filled in first even though $3s_{1/2}$ state is slightly lower (by about 0.31 MeV) than the $1g_{9/2}$ state as has been shown in the lower panel of Fig. 7. Still another addition of 2 neutrons is found to fill in the $1g_{9/2}$ state once again, though now the $1g_{9/2}$ state is higher to the $3s_{1/2}$ state merely by 0.08 MeV. This preference for the $1g_{9/2}$ state stems from the fact that in contrast to the $3s_{1/2}$ state, the positive energy $1g_{9/2}$ state being a resonant state has its wave function entirely confined inside the potential well akin to a bound state as shown earlier in Fig. 2 for the nucleus ^{64}Ca. For the neutron number N = 48, it is found that both the $1g_{9/2}$ and $3s_{1/2}$ states become bound and start to compete together to get occupied on further

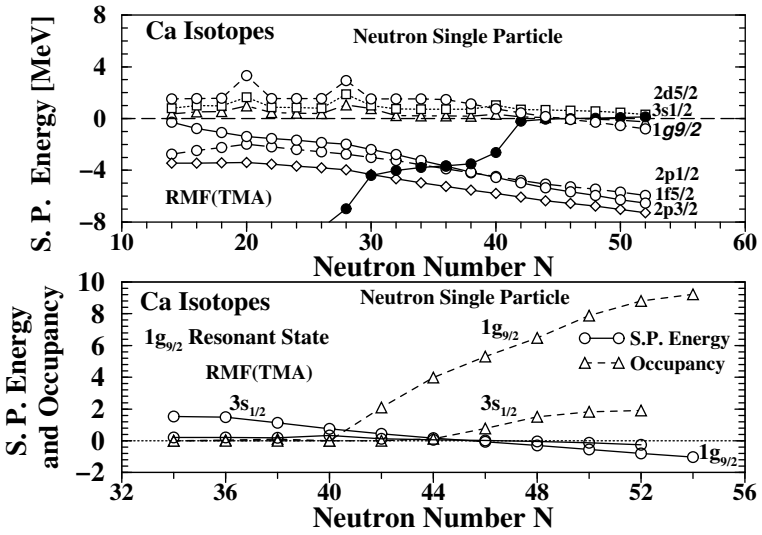

Fig. 7. Upper panel: Variation of the neutron single particle energies obtained with the TMA force for the Ca isotopes with increasing neutron number. The Fermi level has been shown by filled circles connected by solid line to guide the eyes. Lower panel: Variation of the position and occupancy (no. of neutrons occupying the levels) of the neutron $1g_{9/2}$ and $3s_{1/2}$ single particle states in the neutron rich Ca isotopes.

addition of neutrons as can be seen in Fig. 7 (lower panel). Further it is observed from the figure that both of these states are completely filled in for the neutron number N = 52 and, thus, the neutron drip line is reached with a loosely bound ^{72}Ca nucleus. The next single particle state, $2d_{5/2}$, is higher in energy by about 0.5 MeV in the continuum and further addition of neutrons does not produce a bound system.

As mentioned above, the $1g_{9/2}$ state is mainly confined to the potential region, and hence its contribution to the neutron radii is similar to a bound state. In contrast, the $3s_{1/2}$ state which has no centrifugal barrier and, therefore, is spread over large spatial extension contributes substantially to the neutron density distribution at large distances. Due to this reason, for $N > 42$ as the $3s_{1/2}$ state starts being occupied the neutron density distributions develop large tails, and the neutron radii for the neutron rich isotopes ($N > 42$) grow abruptly as has been shown in Figs. 4 and 5. Thus the filling in of the $3s_{1/2}$ single particle state with increasing neutron number in the $^{64-72}$Ca isotopes causes the formation of neutron halos in these nuclei.

It is pertinent to point out that our results described above are consistent with the recent non-relativistic HFB calculations of Bennaceur et al. [4] demonstrating the effects of pairing correlations in the description of weakly bound neutron rich nuclei. The interesting result of these authors [4] is that the pairing correlations in the even-N nuclei, contrary to the case of odd-N nuclei (N being the neutron number) for the zero orbital angular momentum (l = 0) s-state, provide additional binding in a way to halt the unlimited increase in the rms radius as the single particle binding of the s-state tends to be zero. Further, it has also been demonstrated by these

authors [4] that the low lying $l = 0$ continuum states contribute significantly in generating large rms neutron radii of the neutron rich weakly bound nuclei, and that the exact position of l=0 orbital is not crucial for this enhancement.

From our Fig. 7 it is seen that the $3s_{1/2}$ orbital whose positions varies only slightly for the neutron number $N = 12$ to $N = 52$ continues to be close to zero energy, starts being occupied only for $N > 42$. This occupancy generates large increase in the neutron rms radii beyond $N = 42$ as is readily observed in Figs. 4 and 5 for the Ca isotopes. Thus our results are in accord with those of Ref. [4] whereby the occupied $l = 0$ orbital provides a significant increase in the neutron rms radii and, moreover, this increase does not tend to become infinitely large even when the single particle energy of the s-state changes to lie very close to zero. In a similar calculation for deformed nuclei it may be difficult to discuss the results in terms of single particle wave functions as shown in Fig. 1 for the spherical case. However, we believe that the main conclusions drawn here to characterize a favorable situation for the halo formation will not change significantly in a similar description for the even-even deformed nuclei .

4 Conclusion

In conclusion, we have applied the BCS approach using a descretized continuum within the framework of relativistic mean-field theory to study the ground state properties of Ca isotopes up to the drip-lines, the main emphasis being on the possible formation of halos in the neutron rich Ca isotopes. Calculations have been performed using the popular TMA and the NL-SH sets of parameters for the effective mean-field Lagrangian. For the pairing energy a δ-function interaction has been employed for the state dependent BCS calculations. It is found that from amongst the positive energy states, apart from the single particle states adjacent to the Fermi level, the dominant contribution to the pairing correlations is provided by a few states which correspond to low-lying resonances. An important result to be emphasized is the following. In the vicinity of neutron drip-line for the Ca isotopes, it is found that further addition of neutrons causes a rapid increase in the neutron rms radius with a very small increase in the binding energy, indicating thereby the occurrence of halos in the neutron rich Ca isotopes. The filling in of the resonant $1g_{9/2}$ state, that sets in even before it becomes bound, with a very little increase in the binding energy causes the existence of extremely neutron rich Ca isotopes, whereas the occupancy of loosely bound $3s_{1/2}$ state gives rise to the halo formation. Also, as in earlier prototype calculations [30, 31] for the Ni and Sn isotopes, our present RMF+BCS results for the two neutron separation energy, rms neutron and proton radii and pairing energies for the Ca isotopes compare well with the known experimental data [38]. Furthermore, detailed comparisons show that the RMF+BCS approach provide results almost similar to those obtained in the more complete relativistic continuum Hartree Bogoliubov (RCHB) treatment [32]. This is in accord with the conclusion of Grasso et al. [11] whereby the BCS approach is shown to be a good approximation to the Bogoliubov treatment in the context of non-relativistic mean-field studies. Moreover, the effects of pairing correlations observed in our treatment are found to be in agreement with those demonstrated recently by Bennaceur et al. [4] as regards to the contribution of the $l = 0$ orbital angular momentum s-state to the large enhancement of the neutron rms radii, and also to the so called pairing anti-halo effect which prevents the unlimited growth of the neutron rms radii when the single particle energy of the $l = 0$ orbital tends to be zero.

Acknowledgments

One of the authors (HLY)would like to thank Prof. Toki for numerous fruitful discussions. Support through a grant by the Department of Science and Technology(DST), India is also acknowledged. HLY would also like to thank Prof. Faessler for his kind hospitality while visiting Institut für Theoretische Physik der Universität Tübingen, Germany where part of this work was carried out. The authors are indebted to J. Meng for communicating some of his RCHB results before publication.

References

[1] I. Tanihata: *J. Phys. G* **22** (1996) 157 ; I. Tanihata*et al*.: *Phys. Rev. Lett.* **55** (1985) 2676

[2] A. S. Jensen, K. Riisager: *Phys. Lett. B* **480** (2000) 39 and references therein

[3] J. Meng, P. Ring: *Phys. Rev. Lett.* **80** (1998) 460 and references therein

[4] K. Bennaceur, J. Dobaczewski, M. Ploszajczak: *Phys. Lett. B* **496** (2000) 154 and references therein

[5] A. B. Migdal: *J. Nucl. Phys.* **16** (1973) 238

[6] J. Dobaczewski, H. Flocard, J. Treiner: *Nucl. Phys. A* **422** (1984) 103 ; J. Dobaczewski, W. Nazarewicz, T. R. Werner: *Phys. Scr. T.* **56** (1995) 15

[7] J. Terasaki, P.-H. Heenen, H. Flocard, P. Bonche: *Nucl. Phys. A* **600** (1996) 371

[8] J. Dobaczewski, W. Nazarewicz, T. R. Werner, J. F. Berger, C. R. Chinn, J. Decharge: *Phys. Rev. C* **53** (1996) 2809

[9] N. Sandulescu, R. J. Liotta, R. Wyss: *Phys. Lett. B* **394** (1997) 6

[10] N. Sandulescu, N. V. Giai, R. J. Liotta: *Phys. Rev. C* **61** (2000) 061301(R)

[11] M. Grasso, N. Sandulescu, N. V. Giai, R. J. Liotta: *Phys. Rev. C* **64** (2001) 064321

[12] J. D. Walecka: *Ann. Phys. (N.Y.)* **83** (1974) 491

[13] B. D. Serot, J. D. Walecka: *Adv. Nucl. Phys.* **16** (1986) 1

[14] P.-G. Reinhard, M. Rufa, J. Marhun, W. Greiner, J. Friedrich: *Z. Phys. A* **323** (1986) 13

[15] A. Bouyssy, J.-F. Mathiot, N. V. Giai, S. Marcos: *Phys. Rev. C* **36** (1987) 380

[16] P-G Reinhard: *Rep. Prog. Phys.* **52** (1989) 439 and references therein

[17] Y. K. Gambhir, P. Ring, A. Thimet: *Ann. Phys. (N.Y.)* **198** (1990) 132

[18] H. Toki, Y Sugahara, D. Hirata, B. V. Carlson, I. Tanihata: *Nucl. Phys. A* **524** (1991) 633

[19] R. Brockman, H. Toki: *Phys. Rev. Lett.* **68** (1992) 3408

[20] D. Hirata, H. Toki, I. Tanihata, P. Ring: *Phys. Lett. B* **314** (1993) 168

[21] Y. Sugahara, H. Toki: *Nucl. Phys. A* **579** (1994) 557 ; Y. Sugahara: *Ph.D. Thesis, Tokyo Metropolitan University* (1995)

[22] P. Ring: *Prog. Part. Nucl. Phys.* **37** (1996) 193 and references therein

[23] M. M. Sharma, M. A. Nagarajan, P. Ring: *Phys. Lett. B* **312** (1993) 377

[24] J. Meng: *Phys. Rev. C* **57** (1998) 1229

[25] J. Meng: *Nucl. Phys.* **635** (1998) 3

[26] G. A. Lalazissis, D. Vretenar, P. Ring: *Phys. Rev. C* **57** (1998) 2294

[27] S. Mizutori, J. Dobaczewski, G. A. Lalazissis, W. Nazarewicz, P. G. Reinhard: *Phys. Rev. C* **61** (044326) (2000).

[28] J. Leja, S. Gmuca: *Acta Phys. Slov.* **51** (2001) 201

[29] M. Del Estal, M. Contelles, X. Vinas, S. K. Patra: *Phys. Rev. C* **63** (2001) 044321

[30] H. L. Yadav, S. Sugimoto, H. Toki: *Mod. Phys. Lett. A* **17** (2002) 2523 ; preprint, RCNP, Osaka University, Osaka (2001).

[31] H. L. Yadav, U. R. Jakhar, K. C. Agarwal: *Acta Phys. Slov.* **53** (2003) 25

[32] J. Meng, H. Toki, J.Y. Zeng, S. Q. Zhang, S. Q. Zhou: *Phys. Rev. C* **65** (2002) 041302(R)

[33] H. L. Yadav, M. Kaushik, H. Toki, *to be published*

[34] A. M. Lane: *Nuclear Theory*, Benjamin (1964)

[35] P. Ring, P. Schuck: *The Nuclear Many-body Problem*, Springer (1980)

[36] G. F. Bertsch, H. Esbensen: *Ann. Phys. (N.Y.)* **209** (1991) 327

[37] A. B. Migdal: *Theory of Finite Fermi Systems and Applications to Atomic Nuclei*, Interscience, New York (1967)

[38] G. Audi, A. H. Wapstra, C. Thibault: *Nucl. Phys. A* **729** (2003) 337

[39] H. de Vries, C. W. de Jager, C. de Vries: *At. Data Nucl. Data Tables* **36** (1987) 495

[40] C. J. Batty, E. Friedman, H. J. Gils, H. Rebel: *Adv. Nucl. Phys.* **19** (1989) 1